Electronic Supplementary Material (ESI) for Journal of Materials Chemistry A.

Supporting Information

Regulation of the Electronic Structure of Perovskites to Improve the Electrocatalytic Performance for the Nitrogen-reduction Reaction

Chemicals and Materials

Lanthanum nitrate hexahydrate ($La(NO_3)_3·6H_2O$, 99.9%; Aladdin), cobalt nitrate ($Co(NO_3)_2·6H_2O$, 99.9%; Aladdin), nickel nitrate hexahydrate ($Ni(NO_3)_2·6H_2O$, 99.99%; Aladdin), sulfuric acid (H_2SO_4, 98%; Beijing Chemical Works), hydrogen peroxide solution (H_2O_2, AR, 30 wt% in H_2O; Aladdin), potassium chloride (KCl, AR, 99.5%; Aladdin), ammonium sulfate ($(NH_4)_2SO_4$, 99.99%; Aladdin), ammonium sulfate-^{15}N ($(^{15}NH_4)_2SO_4$, 99 atom%, ≥98.5%; Aladdin), N_2 gas (99.999%), Ar gas (99.999%), potassium sulfate (K_2SO_4, AR, 99%; Aladdin), salicylic acid ($C_7H_6O_3$, 99.5%; Macklin), sodium citrate dihydrate ($C_6H_5Na_3O_7·2H_2O$, ≥99.0%; Aladdin), sodium hydroxide (NaOH, AT, 96%; Aladdin), sodium hypochlorite solution (NaClO, available chlorine 4.0%; Macklin), sodium nitroferricyanide dihydrate ($C_5FeN_6Na_2O·2H_2O$, 99.98%; Aladdin), citric acid monohydrate ($C_6H_8O_7·H_2O$, 99.5%; Aladdin), carbon paper (NOS10025; CeTech Taiwan), 5% Nafion solution (Dupont), 212 Nafion membrane (Alfa Aesar) and ultrapure water (Millipore) were purchased. All chemical reagents were used as received.

Experimental Section

Synthesis of Co-LNO

First, 3 mmol of $La(NO_3)_3·6H_2O$, 3 mmol of $Co(NO_3)_2·6H_2O$ and $Ni(NO_3)_2·6H_2O$ (changing Co/Ni ratio according to demand) and 6 mmol of $C_6H_8O_7·H_2O$ were dissolved in a mixed solution of ethanol and water. Then, the obtained solution was evaporated tardily to obtain a gel at 80 °C, and then dried at 120 °C. The obtained powders were calcined at 600 °C for 2 h and then at 800 °C for 4 h, at a heating rate of 1 °C/min. The obtained powders were washed carefully by ultra-pure water repeatedly and then freeze-dried to obtain a series of Co-LNO.

Electrocatalytic nitrogen reduction reaction testing

The Electrocatalytic nitrogen reduction reaction (ENRR) was carried out in a two-compartment H-type electrolytic tank. It contained a Nafion 212 membrane and a three-electrode system (Co-LNO/carbon paper = working electrode; Pt network = counter electrode; Ag/AgCl (saturated KCl solution) = reference electrode). The Nafion membrane was washed in an aqueous solution of 5% H_2O_2 and ultrapure water at 80 ^oC for 1 h sequentially for pretreatment. Co-LNO catalysts (20 mg) were dispersed in a mixture of ethanol (0.99 mL) and 5 wt% Nafion ethyl alcohol (0.01 mL), and alcohol-dispersion liquid (5 μL) was loaded onto carbon paper (1×0.5 cm^2) and dried naturally at room temperature.

Chronoamperometry measurement results were obtained after several cycles of cyclic voltammetry. High-purity N_2 was used to remove the air in the cathodic compartment first. Then, high-purity N_2 was passed continuously while conducting the electrolysis experiment. Chronoamperometry measurements were undertaken in K_2SO_4 (0.01 M) at different potentials. Each test was repeated thrice to ensure the reproducibility of experimental results.

Determination of ammonia and hydrazine

For the indophenol-blue method, according to the method of Liang-Xin Ding and Haihui Wang[1], 2 mL of electrolyte in the cathode (50 mL) was used after chronoamperometry measurements. Then, 1 mL of aqueous NaClO (0.05 M), 2 mL of NaOH solution (1 M) with salicylic acid (5 wt%), sodium citrate (5 wt%) and 0.2 mL of $C_5FeN_6Na_2O$ solution (1 wt%) were added sequentially. After 1 h, the spectrum was surveyed by a UV–Vis spectrophotometer (TU-1900).

For ^{1}H NMR spectroscopy, according to the method of reported article[2], after electrolysis, the electrolyte in the cathode was modified to pH 2–2.5 using concentrated sulfuric acid, and then concentrated. Samples were dissolved in deuterated dimethyl sulfoxide with non-deuterated dimethyl sulfoxide as an internal standard. The obtained solution was tested using a ^{1}H NMR system (NMR 500; Bruker).

Labelled $^{15}N_2$ needs to go through pretreatment, which is sequentially introduced into the HCl solution, KOH solution, pure water, and finally to the cathode of the reaction cell.

We employed the method of Watt and Chrisp to quantify the amount of hydrazine.[3] The developing solution was a mixture of 0.99 g *para*-(dimethylamino) benzaldehyde, 5 mL of concentrated HCI and 50 mL of ethanol. Hydrazine hydrate solution (5 mL) of different known concentrations was mixed with 5 mL of the developing solution. After standing for 10 min, the absorbance of the resultant solution was measured at 457 nm using a UV–Vis spectrophotometer.

Average yield rate of NH_3

$$R_{NH_3} = (C_{NH_3} \times V)/(t \times m_{cat.}) \quad (1)$$

Where C_{NH_3} is the measured concentration (μg mL^{-1}), V is the volume of electrolyte (mL), t is the electrolysis time (h) for the NRR and $m_{cat.}$ is the catalyst loading (mg).

Faradaic efficiency

$$Faradaic\ efficiency = 3F \times C_{NH_3} \times V/(17 \times Q)\ or\ （18 \times Q） \quad (2)$$

Where F is the Faraday constant, Q is the total electricity used during the NRR, 17 is the molar mass of $^{14}NH_3$, and 18 is the molar mass of $^{15}NH_3$.

Energy efficiency

The EE of synthetic NH_3 for Co-LNO materials was computed by the following equation:

$$\Phi_{NH_3} = FE(\%) \times \triangle E^{0}_{NH_3} / \triangle E_{NH_3} \quad (3)$$

Where Φ_{NH_3} represents the EE (%) for the NRR, $\triangle E^{0}_{NH_3}$ represents the potential difference between half reactions of standard water oxidation (1.23 V *vs*. RHE) and the standard reduction of nitrogen to ammonia (0.156 V *vs*. RHE), and $\triangle E_{NH_3}$ represents the potential difference between half reactions for standard water oxidation (1.23 V *vs*. RHE) and the actual applied potential at the cathode for the NRR.[4]

Materials characterization

TEM was undertaken using the G2 S-Twin system (FEI Tecnai). XPS spectroscopy was conducted using the ESCALABMKLL X-ray photoelectron spectrometer (VG Scienta) employing an Al Kα source. An AtomScan Advantage instrument (Thermo Scientific) was employed for ICP-OES. Then, UV–Vis absorbance spectra were obtained on a UV–Vis spectrophotometer (TU-1900; Beijing Purkinje General). Electrochemical experiments were undertaken using the VMP-300 Electrochemical Station (Biologic Science Instruments). N_2-TPD data were obtained on an Autochem II 2920 apparatus (Micrometrics).

Calculation information

The Vienna Ab initio Simulation Package (www.vasp.at/) (including van der Waals (D3) correction) was

considered with spin-polarized DFT employed for all calculations. A cutoff energy of 400 eV for the plane-wave basis set and single gamma-point grid sampling were used for structure optimization and adsorption; 2 × 2 × 1 K-point was employed for electronic-structure calculations. The Perdew–Burke–Ernzerhof (PBE) generalized gradient approximation was chosen to treat the exchange correlation potential. The whole model was based on the (001) plane of Co-$LaNiO_3$, and a vacuum space >15 Å was employed to avoid the interaction to eliminate imaginary interactions. Atomic positions were optimized until the maximum force on each atom was less than −0.03 eV/A and 10^{-5} eV.

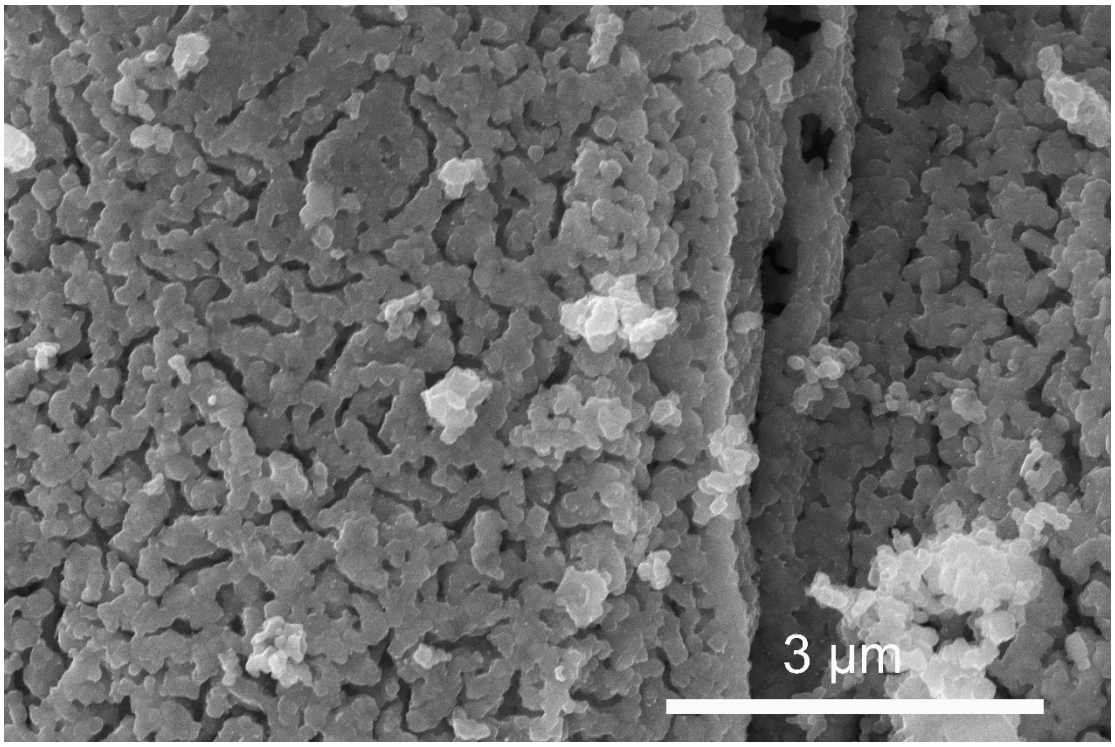

Figure S1. SEM image of Co-LNO-3.

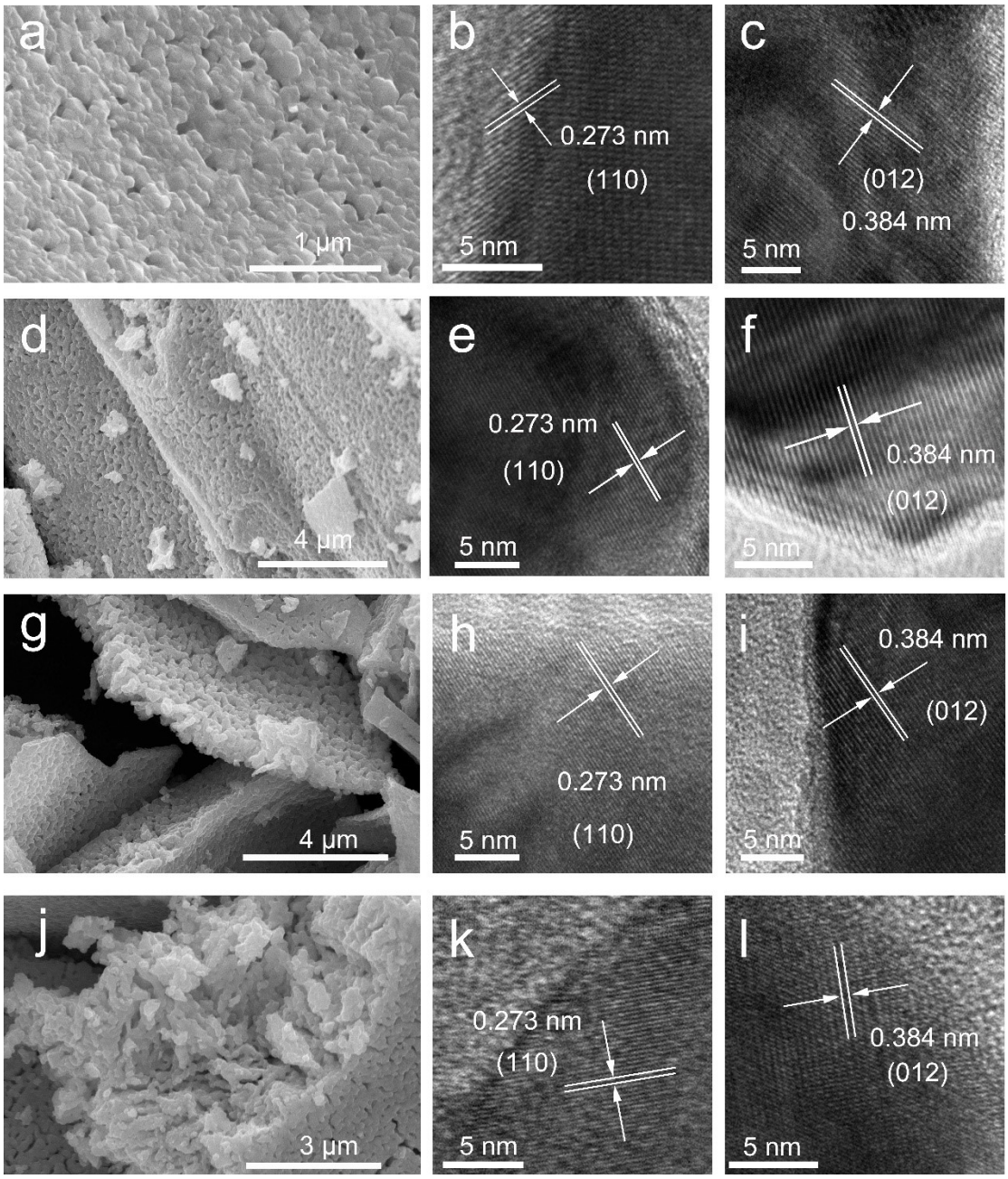

Figure S2. SEM and HRTEM images of a-c, Co-LNO-1; d-f, Co-LNO-2; g-i, Co-LNO-4; j-l, Co-LNO-5.

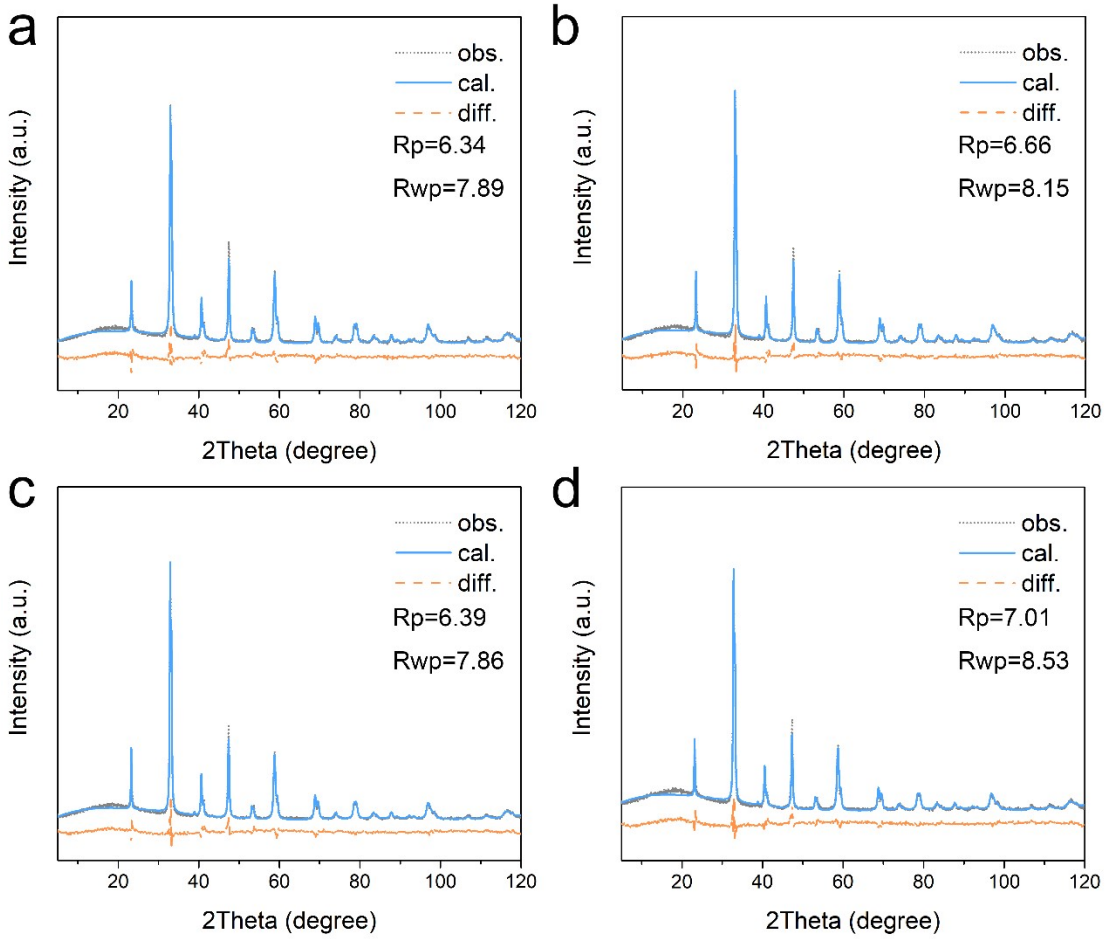

Figure S3. XRD patterns and Rietveld refinements of X-ray diffraction for a, Co-LNO-1; b, Co-LNO-2; c, Co-LNO-4; d, Co-LNO-5.

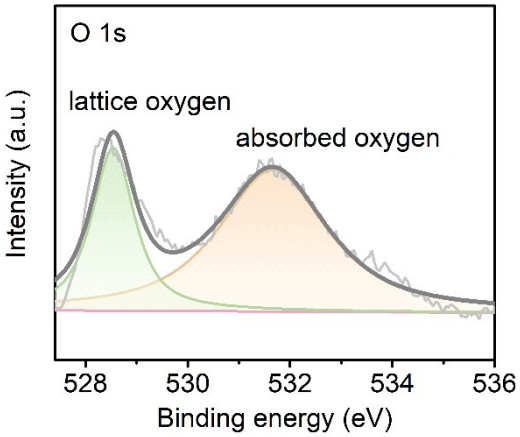

Figure S4. High-resolution XPS spectra of O 1s for Co-LNO-3.

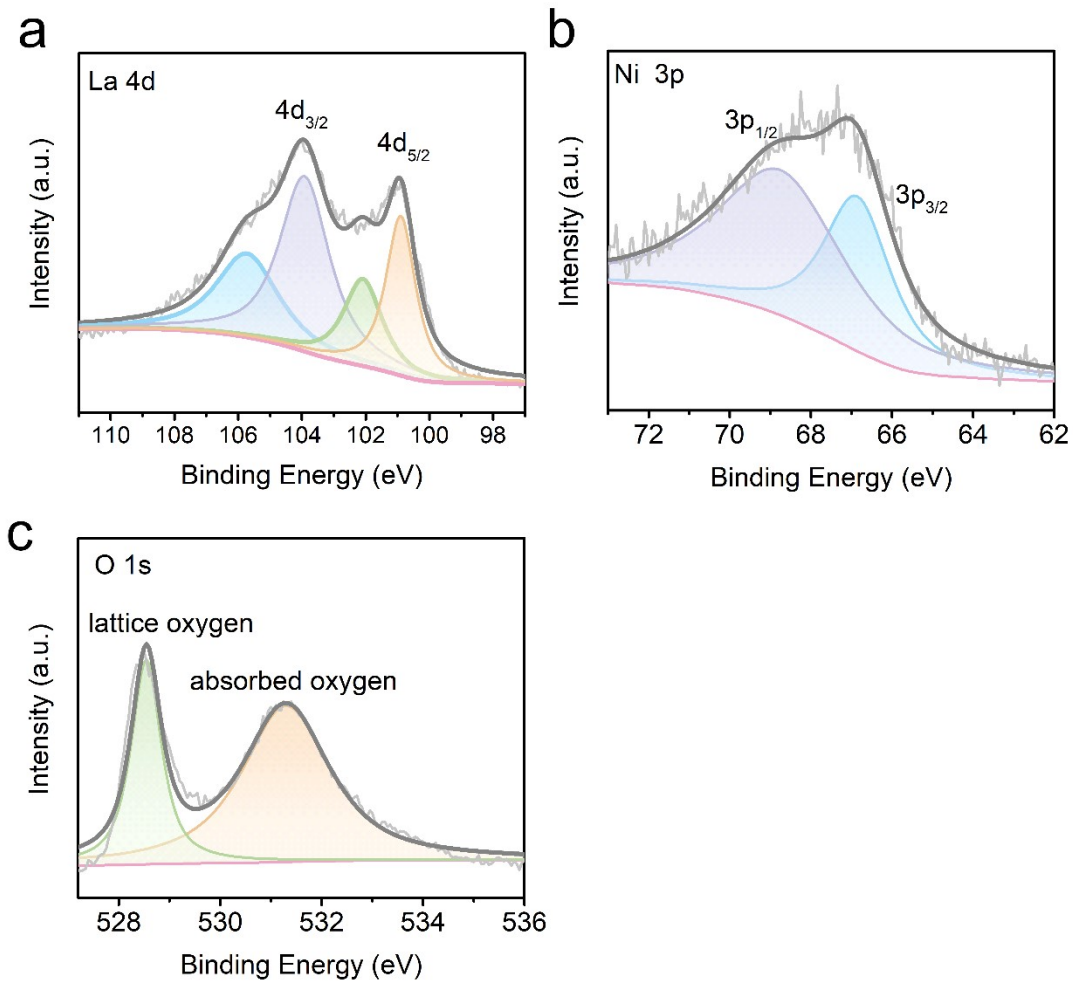

Figure S5. High-resolution XPS spectra of a, La 4d, b, Ni 3p and c, O 1s, of Co-LNO-1.

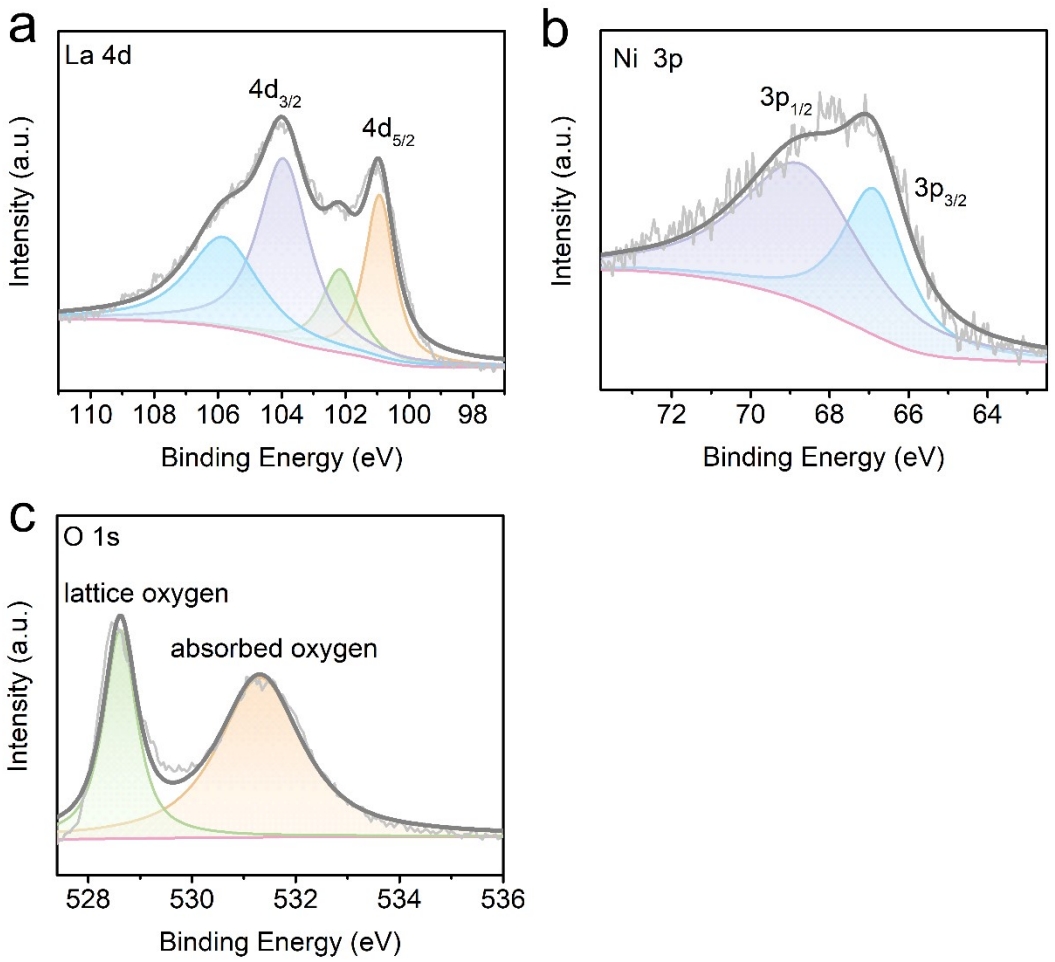

Figure S6. High-resolution XPS spectra of a, La 4d, b, Ni 3p and c, O 1s, of Co-LNO-2.

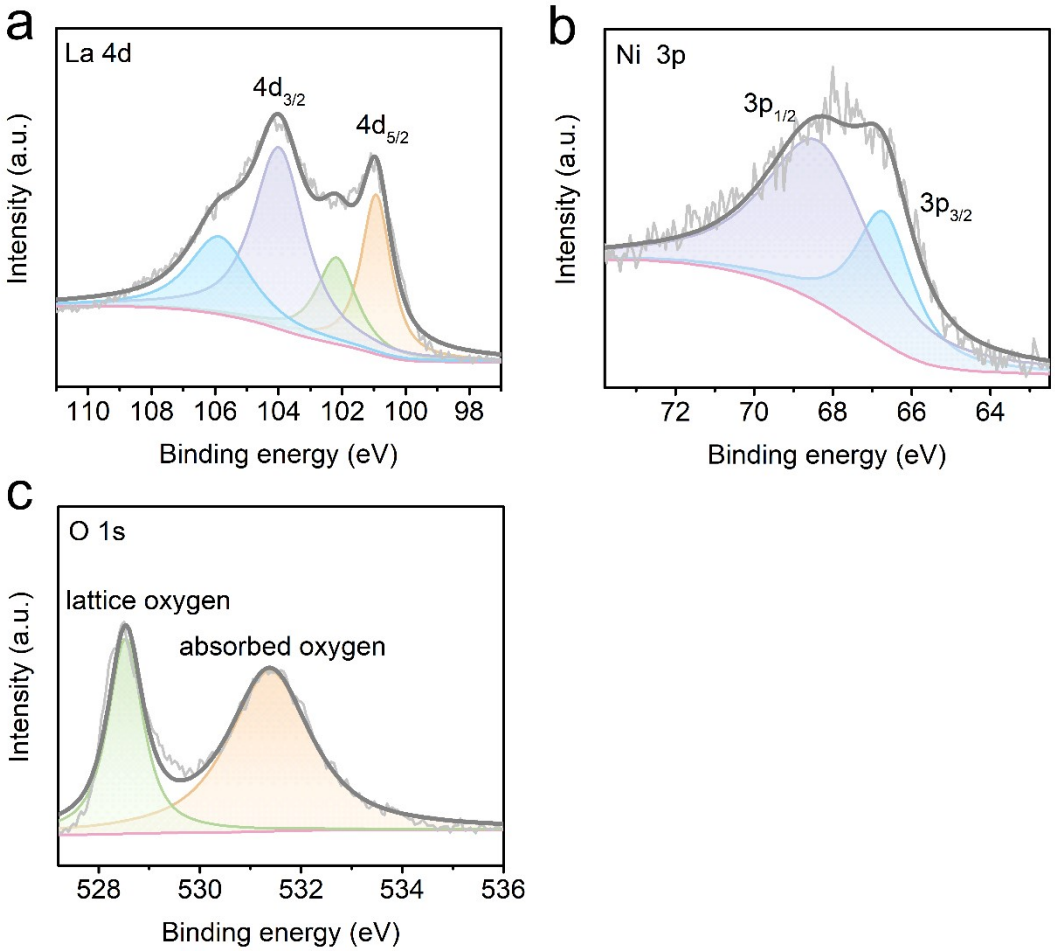

Figure S7. High-resolution XPS spectra of a, La 4d, b, Ni 3p and c, O 1s, of Co-LNO-4.

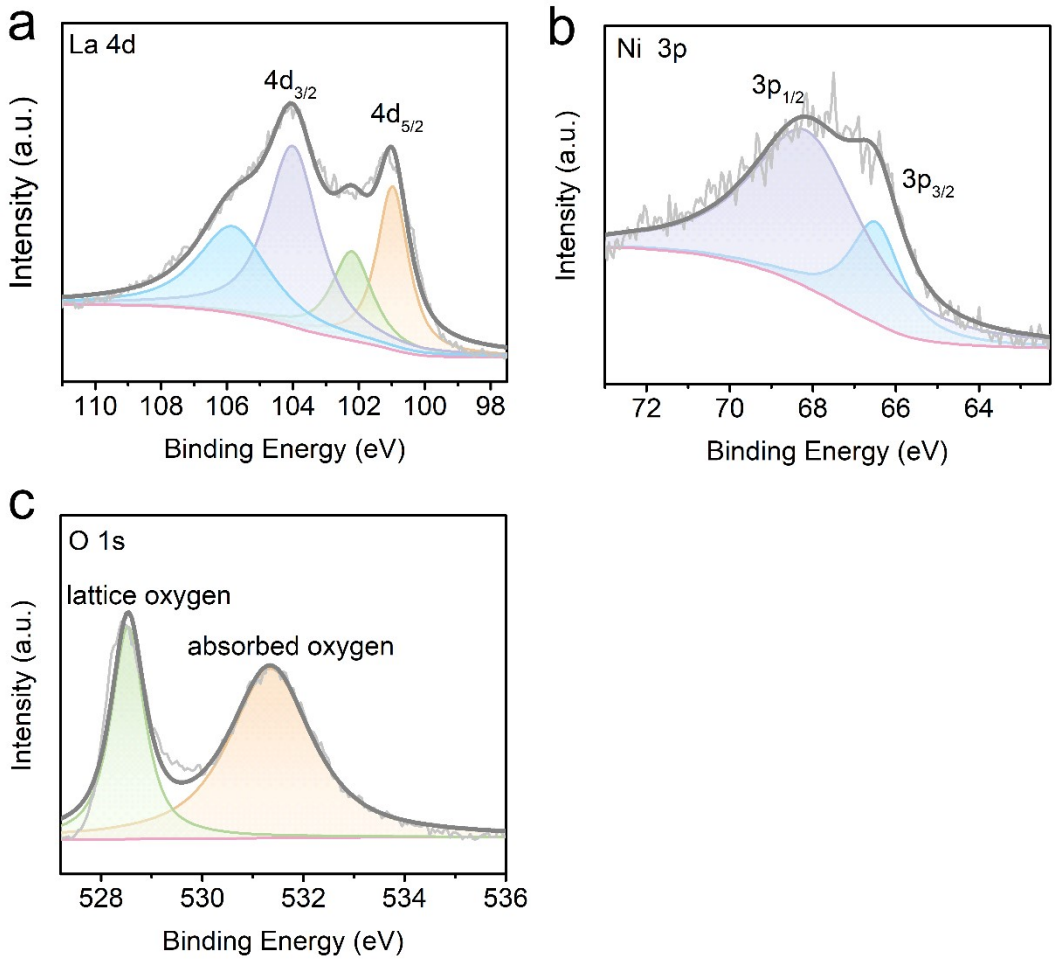

Figure S8. High-resolution XPS spectra of a, La 4d, b, Ni 3p and c, O 1s, of Co-LNO-5.

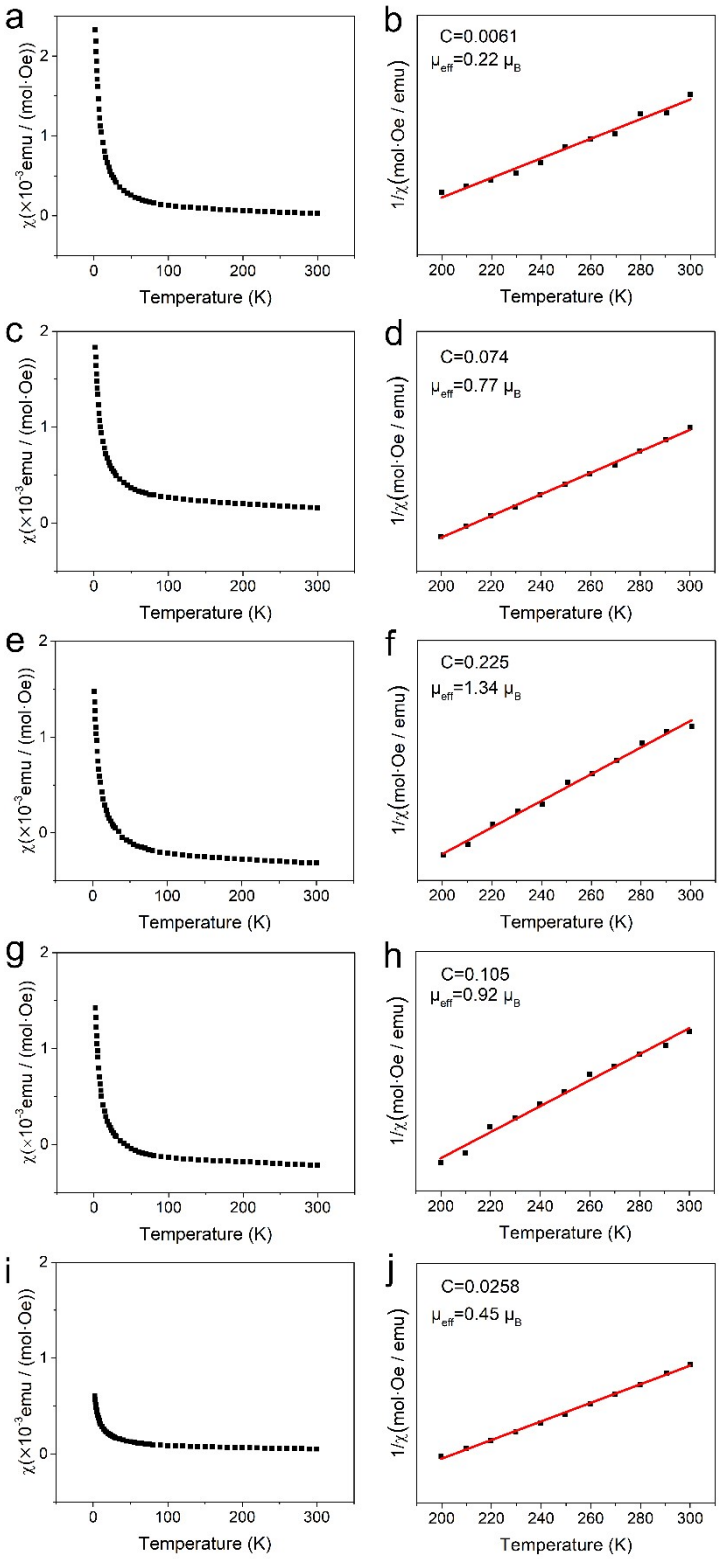

Figure S9. Temperature-dependent magnetic susceptibility χ (a, c, e, g, i) and inverse susceptibility 1/χ (b, d, f, h, j) of, respectively, a and b, Co-LNO-1; c and d, Co-LNO-2; e and f, Co-LNO-3; g and h, Co-LNO-4; i and j, Co-LNO-5.

Curie–Weiss law:

$$\chi = \frac{C}{T - T_c}$$

Where χ is the magnetic susceptibility, C is the Curie constant of the substance, T is the absolute temperature (K) and T_c is the Curie temperature of the substance (K).

$$\mu_{eff} = \sqrt{8C}$$

Where μ_{eff} is the effective magnetic moment and C is the Curie constant of the substance.[5]

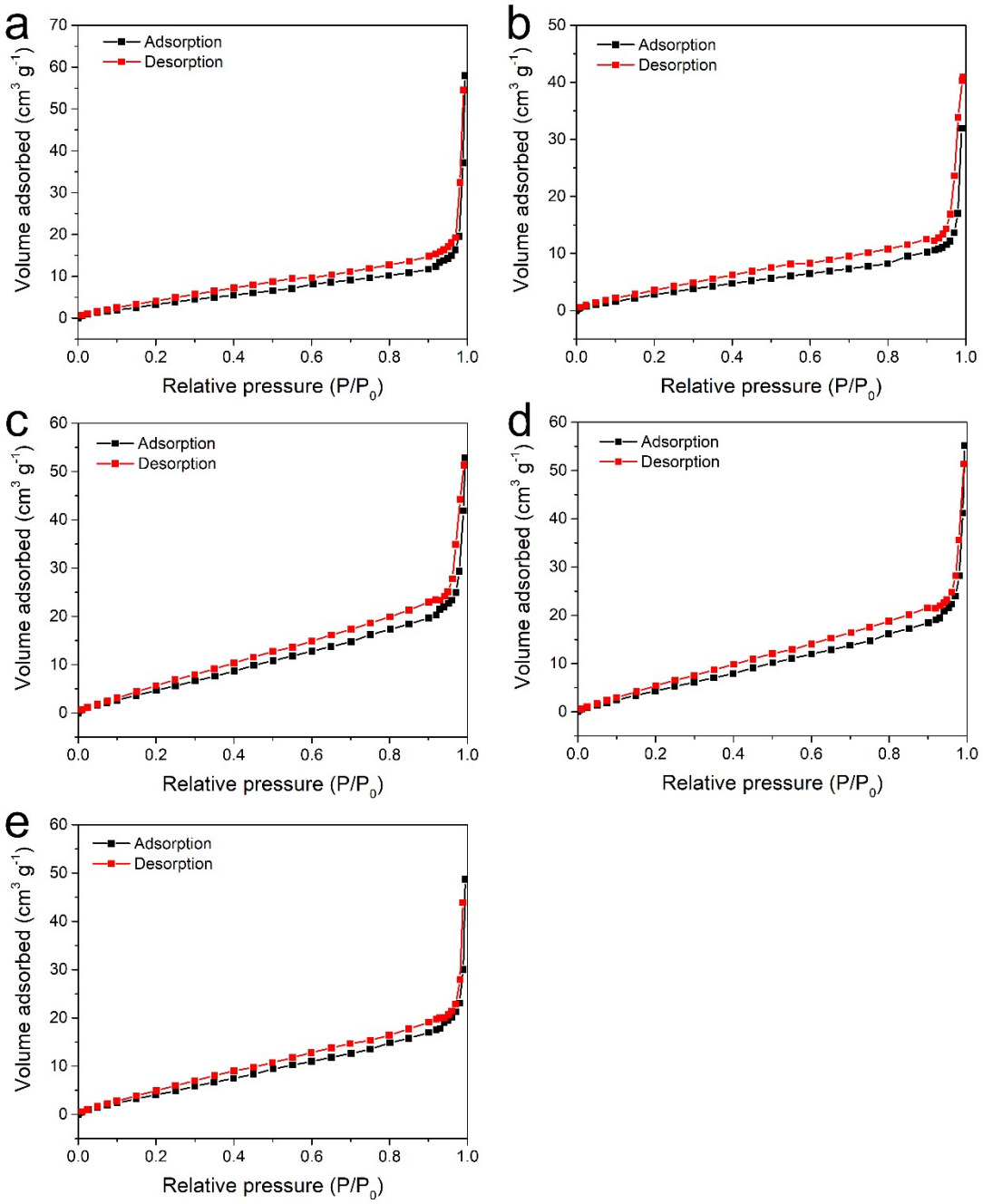

Figure S10. Nitrogen adsorption–desorption isotherms of a, Co-LNO-1; b, Co-LNO-2; c, Co-LNO-3; d, Co-LNO-4; e, Co-LNO-5.

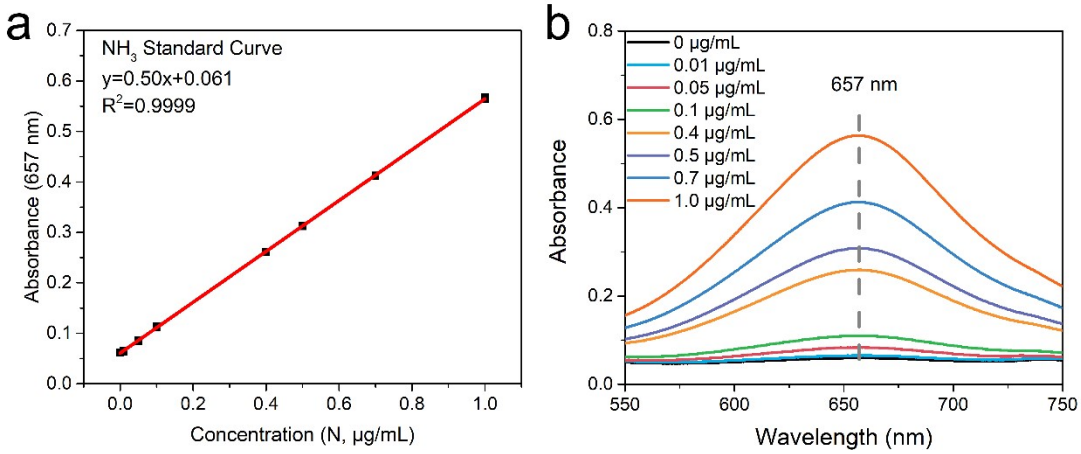

Figure S11. a, Standard curve quantified by the indophenol-blue method using ammonium chloride solutions of known concentration as standards. b, Standard spectra of UV–Vis for different concentration of $N(NH_4^+)$.

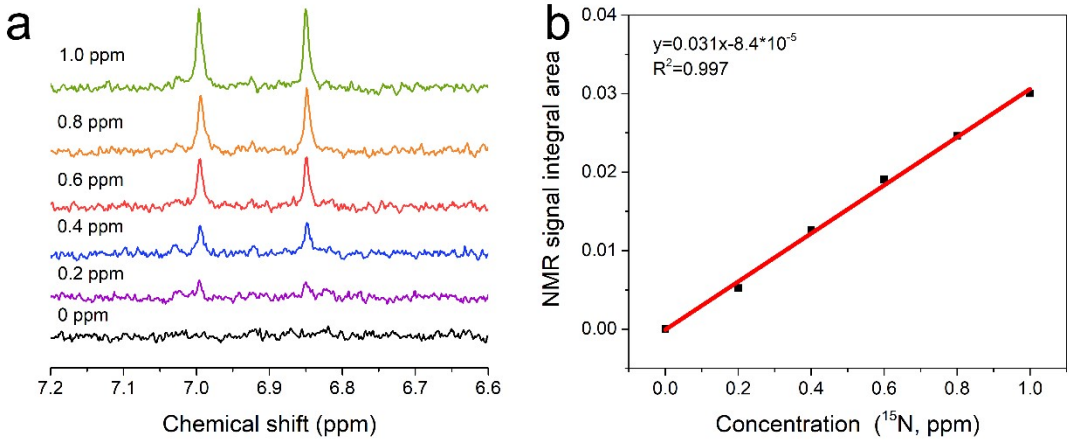

Figure S12. a, ^{1}H-NMR spectra of $^{15}NH_4^+$ and b, standard curves of ^{1}H NMR using a known nitrogen concentration of $^{15}NH_4^+$ standard solutions.

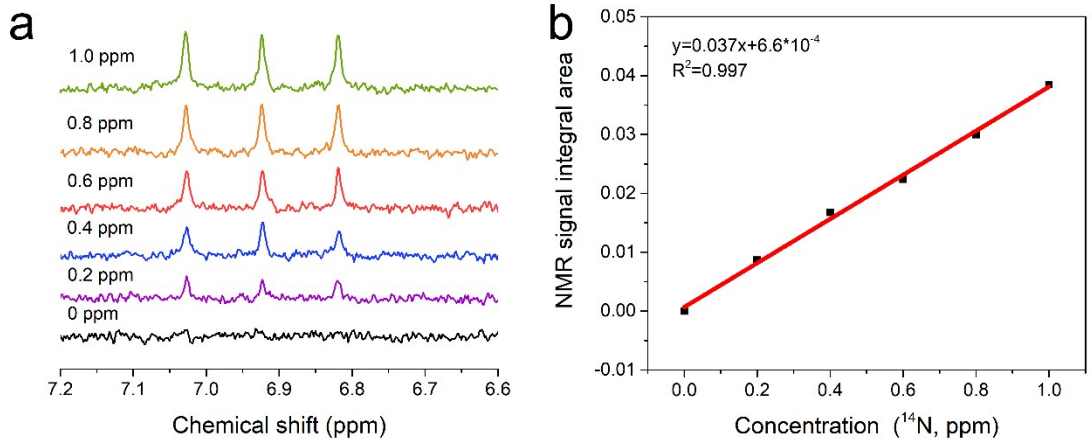

Figure S13. a, ^{1}H-NMR spectra of $^{14}NH_4^+$ and b, standard curves of ^{1}H NMR using a known nitrogen concentration of $^{14}NH_4^+$ standard solutions.

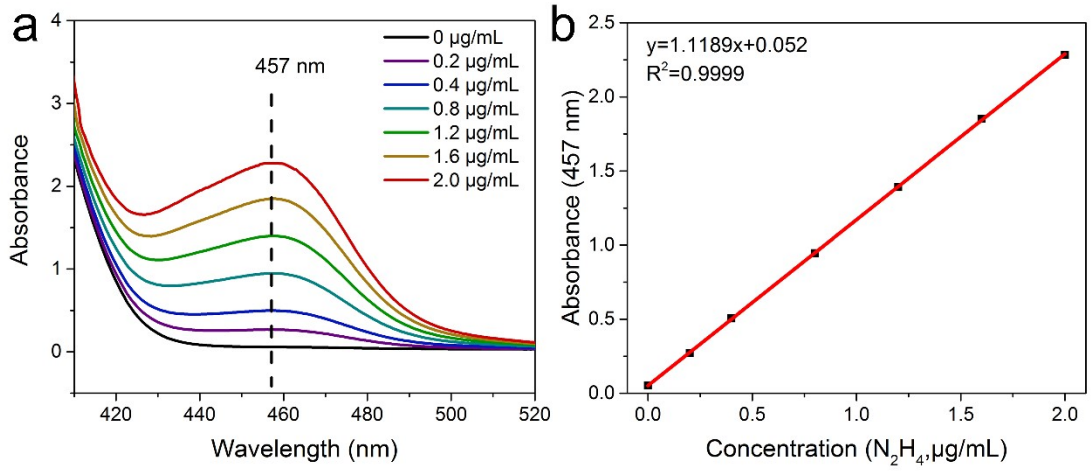

Figure S14. a, UV–Vis curves of various $N_2H_4 \cdot H_2O$ concentrations after incubation for 10 min at room temperature. b, Standard curve quantified by the Watt and Chrisp method for estimating the $N_2H_4 \cdot H_2O$ concentration.

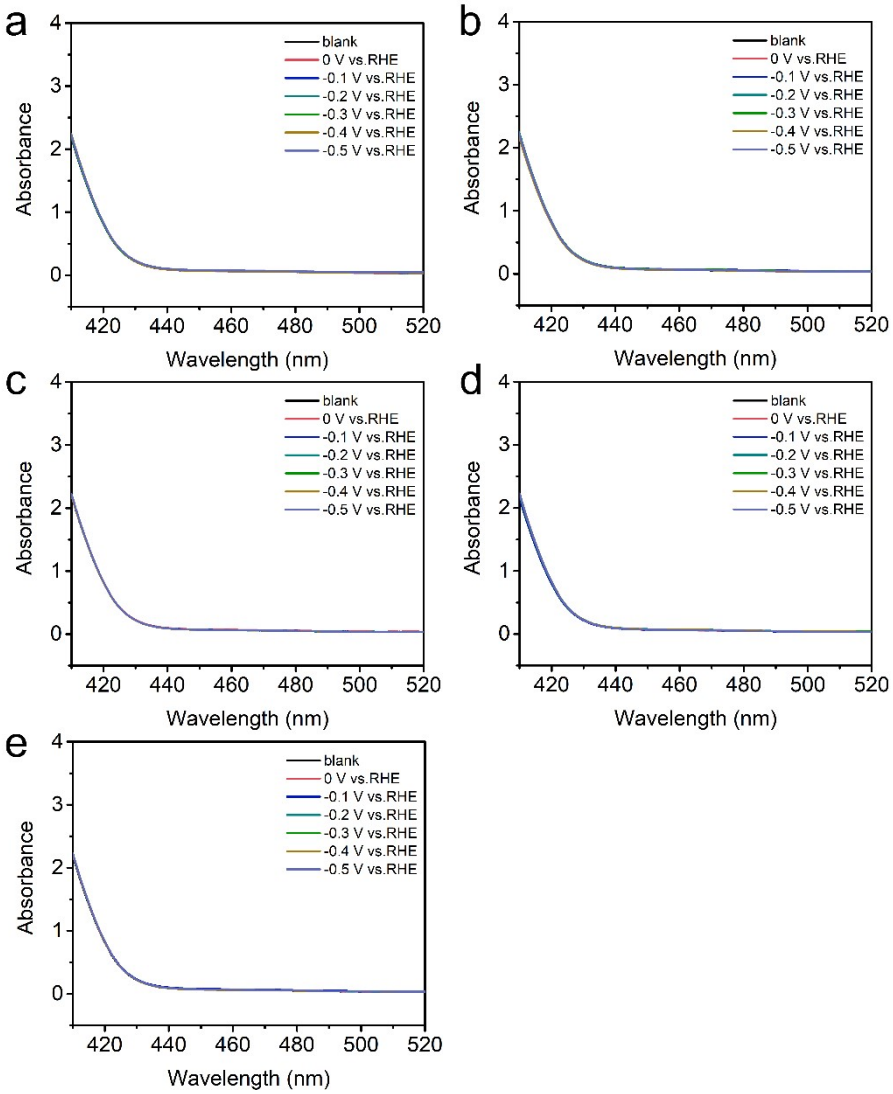

Figure S15. UV–vis absorption spectra of an electrolytic solution after electrolysis at different potentials using a, Co-LNO-1, b, Co-LNO-2, c, Co-LNO-3, d, Co-LNO-4, and e, Co-LNO-5 as catalysts to quantify hydrazine hydrate.

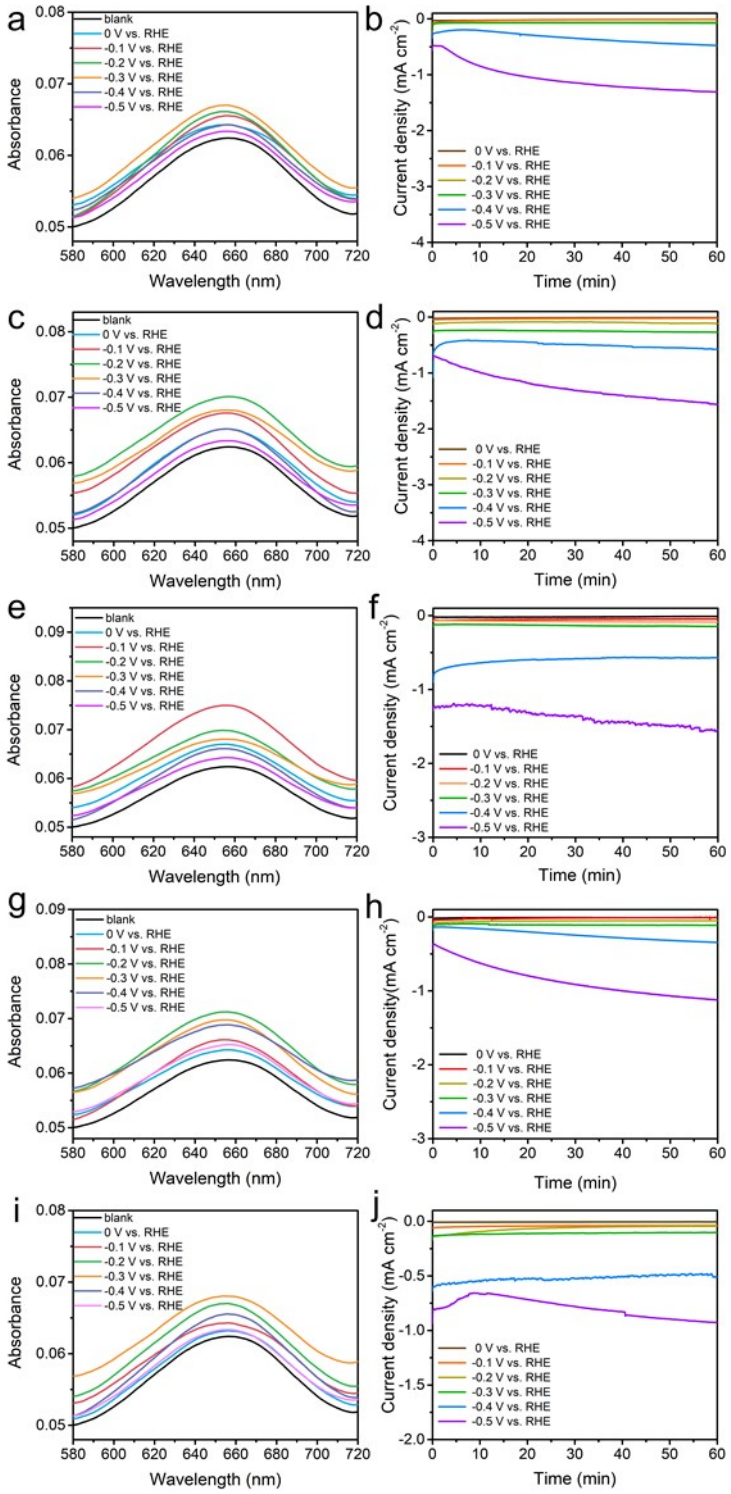

Figure S16. UV–vis absorption spectra of electrolytes after electrolysis and chronoamperometry curves at different potentials using a and b, Co-LNO-1, c and d, Co-LNO-2, e and f, Co-LNO-3, g and h, Co-LNO-4 and i and j, Co-LNO-5 as catalysts.

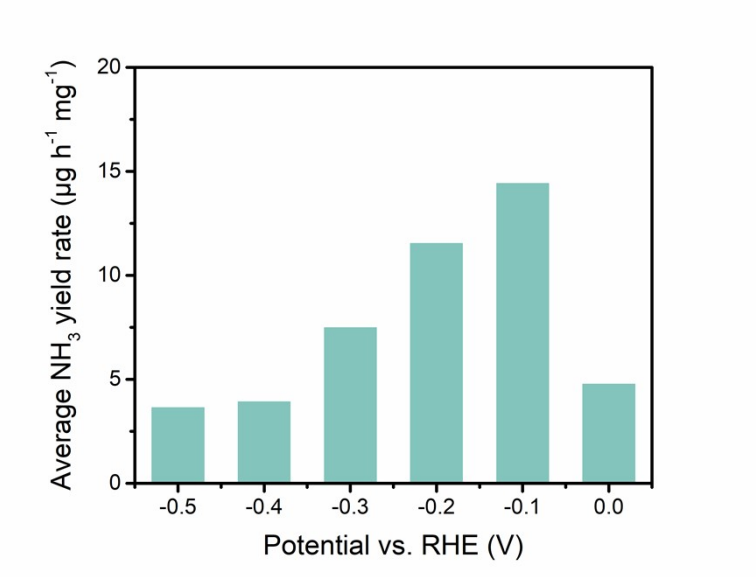

Figure S17. Average rate of NH_3 produced of Co-LNO-3 quantified by ^{1}H NMR with $^{14}N_2$ feeding.

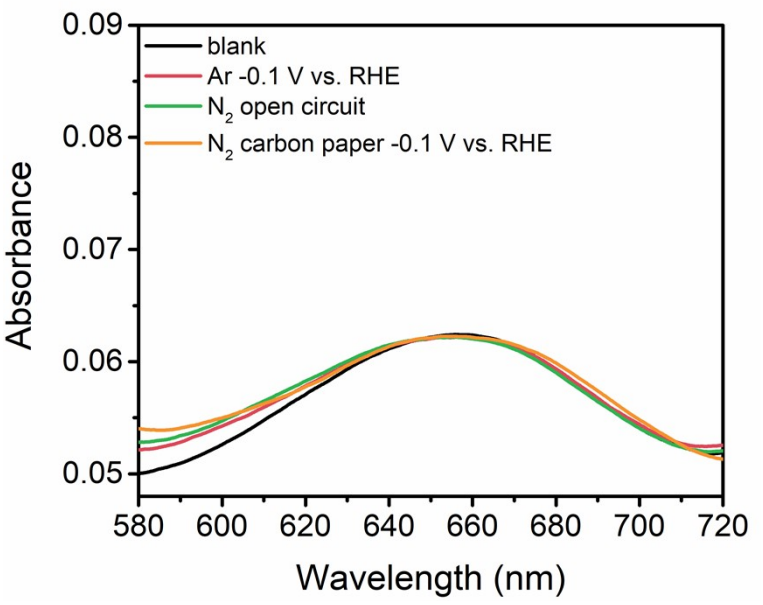

Figure S18. UV–Vis absorption spectra of control experiments. Co-LNO-3 was used as a catalyst in control experiments with Ar feeding at a potential of −0.1 V *vs*. RHE and with N_2 feeding under open circuit.

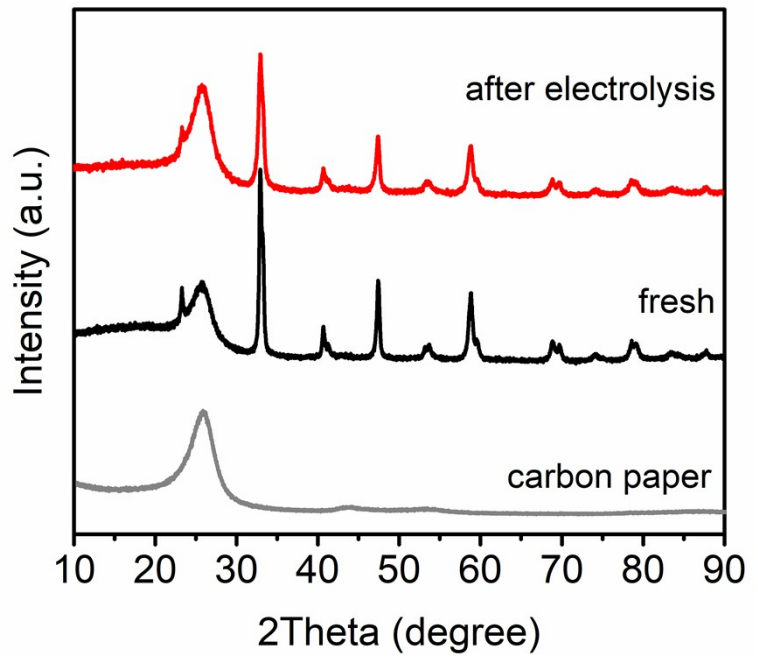

Figure S19. Comparison of XRD patterns of Co-LNO-3 on carbon paper before and after 90 h of electrolysis at a potential of −0.1 V, and the carbon paper.

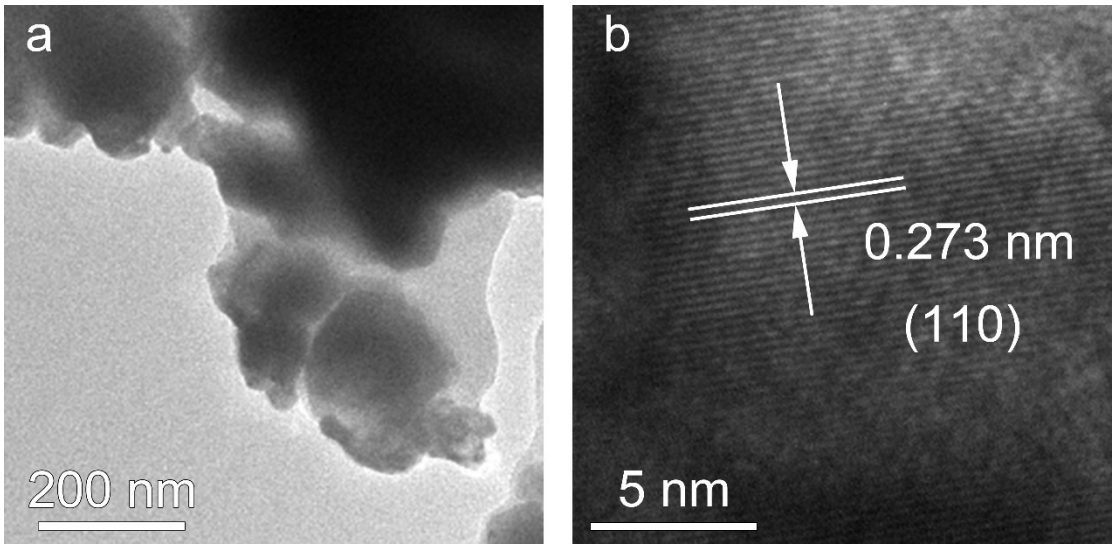

Figure S20. TEM and HRTEM images of Co-LNO-3 after 90 h of electrolysis at a potential of −0.1 V.

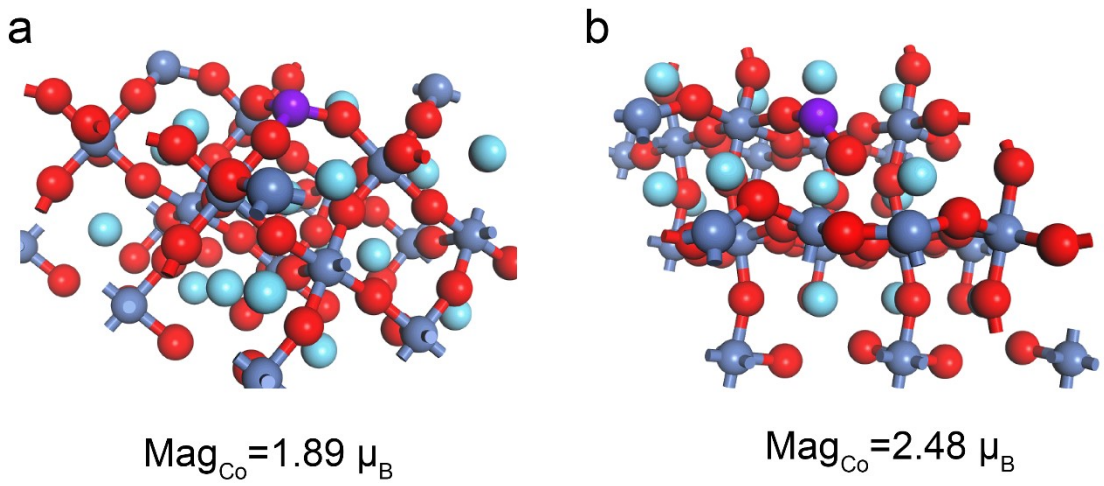

Figure S21. Ball-and-stick model of a, Co-LNO and b, OV-Co-LNO, and the corresponding calculated spin magnetic moment of Co sites. Red, O; light-blue, La; gray-blue, Ni; purple, Co.

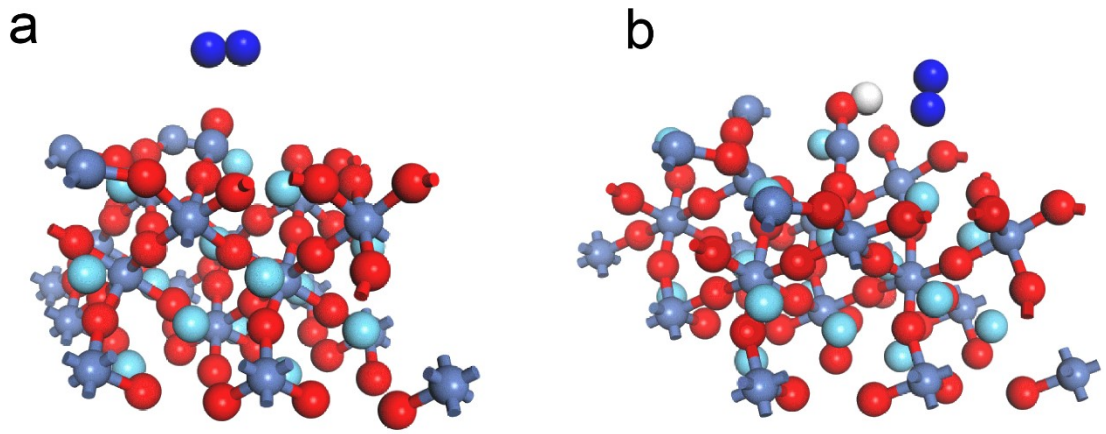

Figure S22. Ball-and-stick model of *NN adsorption on a Ni site of a, OV-LNO and b, the model after the first hydrogenation on the Ni site of OV-LNO. Red, O; light-blue, La; gray-blue, Ni; bright-blue, N; light gray, H.

Table S1. The metal-element feed ratios, determination of metal-element ratios obtained by ICP-OES and surface-area data from Brunauer–Emmett–Teller (BET) calculations of Co-LNO materials

Catalyst	Co/La (feed atomic ratio)	Co/La (atomic ratio by ICP-OES)	BET (g/cm^2)
Co-LNO-1	0.001	0.0013	17.8
Co-LNO-2	0.003	0.0032	15.95
Co-LNO-3	0.005	0.0047	29.04
Co-LNO-4	0.007	0.0065	27.68
Co-LNO-5	0.01	0.0099	24.66

Table S2. Lattice parameters of Co-LNO materials by Rietveld refinement after X-ray diffraction

Catalyst	Space group	Cell parameter/Å, °				
		a = b	c	α	β	γ
Co-LNO-1	RC	5.4599	13.1764	90	90	120
Co-LNO-2	RC	5.4592	13.1835	90	90	120
Co-LNO-3	RC	5.4569	13.1788	90	90	120
Co-LNO-4	RC	5.4583	13.1832	90	90	120
Co-LNO-5	RC	5.4577	13.1787	90	90	120

Table S3. Comparison the NRR performances of Co-LNO-3 catalyst with other catalysts reported at room temperature and atmospheric pressure.

Catalyst	Electrolyte	NH_3 yield	FE	Ref.
Co-LNO-3	0.01 M K_2SO_4	14.57 μg h^{-1} mg^{-1}	26.44%	This work
C-TixOy/C	0.1 M $LiClO_4$	14.8 μg h^{-1} mg^{-1}	17.8%	[6]
$CoFe_2O_4$	0.1 M Na_2SO_4	4.2×10^{-11} mol s^{-1} cm^{-2}	6.2%	[7]
VN/CC	0.1 M HCl	15.56 μg h^{-1} mg^{-1}	3.58%	[8]
MoS_2–rGO	0.1 M $LiClO_4$	24.82 μg h^{-1} mg^{-1}	4.56%	[9]
Sn/SnS_2	0.1 M PBS	23.8 μg h^{-1} mg^{-1}	3.4%	[10]
Mo-FeP	0.1 M HCl	13.1 μg h^{-1} mg^{-1}	7.49%	[11]
Te-C	0.1 M KOH	1.91 $mgh^{-1}cm^{-2}$	4.67%	[12]
MoS_2	0.1 M Na_2SO_4	8.08×10^{-11} mol·s^{-1}·cm^{-2}	1.17%	[13]
Au/CoO_x	0.05 M H_2SO_4	15.1 μg·cm^{-2}·h^{-1}	19%	[14]
$Bi_4V_2O_{11}/CeO_2$	0.1 M HCl	23.21 μg h^{-1} $mg_{cat.}^{-1}$	10.16%	[15]
Bi NPs@CRs	0.1 M HCl	20.80 μg h^{-1} $mg_{cat.}^{-1}$	11.50%	[16]
Co_4N/Co_2C@rGO	0.1 M HCl	24.12 μg h^{-1} $mg_{cat.}^{-1}$	24.97%	[17]
Fe_{SA}-NO-C	0.1 M HCl	31.9 μg h^{-1} $mg_{cat.}^{-1}$	11.8%	[18]
W-NO/NC	0.5 m $LiClO_4$	12.62 μg h^{-1} $mg_{cat.}^{-1}$	8.35%	[19]
Fe-$(O\text{-}C_2)_4$	0.1 M KOH	32.1 μg h^{-1} $mg_{cat.}^{-1}$	29.3%	[20]
FL-BP NSs	0.01 M HCl	31.37 μg h^{-1} $mg_{cat.}^{-1}$	5.07%	[21]

References

[1] H. Cheng, P. Cui, F. Wang, L. X. Ding, H. Wang, *Angew. Chem. Int. Ed. Engl.* 2019, ***58,*** 15541.

[2] Y. Wang, M. M. Shi, D. Bao, F. L. Meng, Q. Zhang, Y. T. Zhou, K. H. Liu, Y. Zhang, J. Z. Wang, Z. W. Chen, D. P. Liu, Z. Jiang, M. Luo, L. Gu, Q. H. Zhang, X. Z. Cao, Y. Yao, M. H. Shao, Y. Zhang, X. B. Zhang, J. G. Chen, J. M. Yan, Q. Jiang, *Angew. Chem. Int. Ed. Engl.* **2019**, *58*, 9464.

[3] G. W. Watt and J. D. Chrisp, *Anal. Chem.* 1952, **24**, 2006.

[4] D. D. Zhu, J. L. Liu and S. Z. Qiao, *Adv. Mater.* 2016, **28**, 3423.

[5] Y. Guo, Y. Tong, P. Chen, K. Xu, J. Zhao, Y. Lin, W. Chu, Z. Peng, C. Wu and Y. Xie, *Adv. Mater.* 2015, **27**, 5989.

[6] Q. Qin, Y. Zhao, M. Schmallegger, T. Heil, J. Schmidt, R. Walczak, G. Gescheidt-Demner, H. Jiao and M. Oschatz, *Angew. Chem. Int. Ed. Engl.* 2019, **58**, 13101.

[7] M. I. Ahmed, S. Chen, W. Ren, X. Chen and C. Zhao, *Chem. Commun.* 2019, ***55,*** 12184.

[8] X. Zhang, R. M. Kong, H. Du, L. Xia and F. Qu, *Chem. Commun.* 2018, ***54***, 5323.

[9] X. Li, X. Ren, X. Liu, J. Zhao, X. Sun, Y. Zhang, X. Kuang, T. Yan, Q. Wei and D. Wu, *J. Mater. Chem. A* 2019, ***7***, 2524.

[10] P. Li, W. Fu, P. Zhuang, Y. Cao, C. Tang, A. B. Watson, P. Dong, J. Shen and M. Ye, *Small* 2019, e1902535.

[11] Y.-X. Luo, W.-B. Qiu, R.-P. Liang, X.-H. Xia and J.-D. Qiu, *ACS Appl. Mater. Interfaces* 2020, ***12***, 17452.

[12] Y. Yang, L. Zhang, Z. Hu, Y. Zheng, C. Tang, P. Chen, R. Wang, K. Qiu, J. Mao, T. Ling and S. Z. Qiao, *Angew. Chem. Int. Ed. Engl.* 2020, ***59***, 4525.

[13] L. Zhang, X. Ji, X. Ren, Y. Ma, X. Shi, Z. Tian, A. M. Asiri, L. Chen, B. Tang and X. Sun, *Adv. Mater.* 2018, e1800191.

[14] Y. Li, J. Zheng, Y. Lyu, M. Qiao, J. P. Veder, R. D. Marco, J. Bradley, R. Wang, A. Huang, S. P. Jiang, S. Wang, *Angew. Chem. Int. Ed. Engl.* 2019, ***58***, 18604.

[15] C. Lv, C.-H. Yan, G. Chen, Y. Ding, J.Sun , Y.Zhou and G.-H. Yu, *Angew. Chem. Int. Ed. Engl.* 2018, ***57,*** 6073.

[16] F. Wang, L. Zhang, T. Wang, F. Zhang, Q. Liu, H. Zhao, B. Zheng, J. Du and X. Sun, *Inorg Chem* 2021, ***60,*** 7584.

[17] H. Qiao, J. Yu, J. Lu, H. Bai, H. Liu, J. Hu, H. Huang and B. Wen, *ACS Sustainable. Chem. Eng.* 2021, ***9,*** 1373.

[18] Y. Li, J. Li, J. Huang, J. Chen, Y. Kong, B. Yang, Z. Li, L. Lei, G. Chai, Z. Wen, L. Dai and Y. Hou, *Angew. Chem. Int. Ed. Engl.* 2021, ***60,*** 9078.

[19] Y. Gu, B. Xi, W. Tian, H. Zhang, Q. Fu and S. Xiong, *Adv. Mater.* 2021, 2100429.

[20] H. Zhao, S. Zhang, M. Jin, T. Shi, M. Han, Q. Sun, Y. Lin, Z. Ding, L. R. Zheng, G. Wang, Y. Zhang and H. Zhang, *Angew. Chem. Int. Ed. Engl.* 2020,**132**, 13525

[21] L. Zhang, L. X. Ding, G. F. Chen, X. Yang and H. Wang, *Angew. Chem. Int. Ed. Engl.* 2019, ***58***, 2612.